Compositional complexity of rods and rings

Cara R. Schiavon[a], Maxwell E. Griffin[a], Marinella Pirozzi[b], Raman Parashuraman[b], Wei Zhou[c], H. A. Jinnah[d], Daniel Reines[e], and Richard A. Kahn[e,*]

[a]Cancer Biology Graduate Program, Graduate Division of Biomedical and Biological Sciences, Laney Graduate School, Atlanta, GA 30307; [b]EuroBioImaging Facility, Institute of Protein Biochemistry, 80131 Naples, Italy; [c]Department of Hematology and Medical Oncology, [d]Department of Neurology and Human Genetics, and [e]Department of Biochemistry, Emory University School of Medicine, Atlanta, GA 30322

ABSTRACT **Rods and rings (RRs) are large linear- or circular-shaped structures typically described as polymers of IMPDH (inosine monophosphate dehydrogenase). They have been observed across a wide variety of cell types and species and can be induced to form by inhibitors of IMPDH. RRs are thought to play a role in the regulation of de novo guanine nucleotide synthesis; however, the function and regulation of RRs is poorly understood. Here we show that the regulatory GTPase, ARL2, a subset of its binding partners, and several resident proteins at the endoplasmic reticulum (ER) also localize to RRs. We also have identified two new inducers of RR formation: AICAR and glucose deprivation. We demonstrate that RRs can be disassembled if guanine nucleotides can be generated by salvage synthesis regardless of the inducer. Finally, we show that there is an ordered addition of components as RRs mature, with IMPDH first forming aggregates, followed by ARL2, and only later calnexin, a marker of the ER. These findings suggest that RRs are considerably more complex than previously thought and that the function(s) of RRs may include involvement of a regulatory GTPase, its effectors, and potentially contacts with intracellular membranes.**

Monitoring Editor
Anne Spang
University of Basel

Received: May 3, 2018
Revised: Jul 12, 2018
Accepted: Jul 13, 2018

INTRODUCTION

The reversible formation of protein aggregates is increasingly understood to be important for a number of normal cellular processes, as well as pathological ones. Such aggregates form as a result of homopolymerization of a single protein or they can contain much greater complexity in composition and size (Aguilera-Gomez and Rabouille, 2017). Such aggregates can be quite large and share the features of an organelle (e.g., the nucleolus, Cajal bodies, P-bodies, U-bodies, eisosomes, purinosomes, G-bodies, loukomasomes, cytoophidia, and rods and rings [RRs]). The functions of some complexes are known, such as assembly of ribosomes or spliceosomes at the nucleolus and Cajal bodies, respectively (Hebert and Poole, 2017; Nunez Villacis *et al.*, 2018), or sites of RNA metabolism (P-bodies [Luo *et al.*, 2018]), while others are less well-understood.

RRs are large, linear- or circular-shaped structures observable in a variety of mammalian cell lines under normal growth conditions and inducible in all cell lines tested (Willingham *et al.*, 1987; Ji *et al.*, 2006; Gunter *et al.*, 2008; Noree *et al.*, 2010; Ramer *et al.*, 2010; Carcamo *et al.*, 2011). RR induction is typically accomplished using the IMPDH (inosine monophosphate dehydrogenase) inhibitors mycophenolic acid (MPA) or ribavirin, which cause a rapid increase in the number and size of RRs (Ji *et al.*, 2006; Carcamo *et al.*, 2011; Thomas *et al.*, 2012; Keppeke *et al.*, 2016). RRs were first formally described following the observation that patients being treated for chronic hepatitis C infection with a combination of ribavirin and interferon α developed autoantibodies against structures, later named RRs (Covini *et al.*, 2012; Keppeke *et al.*, 2012). Such autoantibodies were found to react with IMPDH (Carcamo *et al.*, 2011; Seelig *et al.*, 2011), the rate-limiting enzyme in guanine nucleotide de novo synthesis that catalyzes the conversion of inosine monophosphate (IMP) to xanthosine monophosphate (XMP). IMPDH is by far the most commonly identified component of RRs, and thus the presence of IMPDH and induction in response to IMPDH inhibition are the hallmarks of RRs (Carcamo *et al.*, 2014; Calise *et al.*, 2015).

This article was published online ahead of print in MBoC in Press (http://www.molbiolcell.org/cgi/doi/10.1091/mbc.E18-05-0274) on July 19, 2018.

*Address correspondence to: Richard A. Kahn (rkahn@emory.edu).

Abbreviations used: AICAR, 5-aminoimidazole-4-carboxamide ribonucleotide; CTPS, CTP synthetase; DON, 6-diazo-5-oxo-l-norleucine; ER, endoplasmic reticulum; HGprt, hypoxanthine-guanine phosphoribosyltransferase; IMPDH, inosine monophosphate dehydrogenase; LND, Lesch–Nyhan disease; MPA, mycophenolic acid; RR, rods and rings.

Cytoophidia are also large protein complexes linked to nucleotide metabolism and share a number of similarities with RRs (Gou *et al.*, 2014; Aughey and Liu, 2015; Chang *et al.*, 2015; Liu, 2016). The best established component of cytoophidia is CTP synthetase (CTPS; Ingerson-Mahar *et al.*, 2010; Noree *et al.*, 2010; Carcamo *et al.*, 2011; Liu, 2011), which catalyzes the conversion of uridine triphosphate (UTP) to cytidine triphosphate (CTP). Glutamine is a necessary cofactor in this reaction and glutamine analogues such as 6-diazo-5-oxo-l-norleucine (DON) and acivicin inhibit CTPS, leading to the formation of cytoophidia (Carcamo *et al.*, 2011; Calise *et al.*, 2014; Keppeke *et al.*, 2015a). These drugs also induce the formation of IMPDH-positive RRs (Carcamo *et al.*, 2011; Calise *et al.*, 2014; Keppeke *et al.*, 2015b). Indeed, there is evidence of partial overlap between CTPS-positive and IMPDH-positive structures (Carcamo *et al.*, 2011; Keppeke *et al.*, 2015b) and these terms are sometimes used interchangeably. However, this overlap is not universal and IMPDH inhibitors do not induce the formation of CTPS-positive structures (Keppekee *et al.*, 2015b). For clarity, we will refer to IMPDH-positive structures as RRs and CTPS-positive structures as cytoophidia.

The function of RRs is unclear and even controversial. Because they are strongly induced upon inhibition of guanine nucleotide biosynthesis, a treatment expected to reduce the guanine nucleotide pool, RR formation has been thought of as a cellular response intended to increase guanine nucleotide synthesis (Carcamo *et al.*, 2014). However, a recent study provided strong evidence that oligomerization of IMPDH does not change the enzymatic properties of the enzyme (Anthony *et al.*, 2017). IMPDHs are abundant, soluble proteins that are normally found as tetramers (Gilbert *et al.*, 1979) or octamers (Whitby *et al.*, 1997). There are two isoforms of IMPDH in mammals, IMPDH1 and 2, which share 84% identity in primary sequence. Both are capable of converting IMP to XMP as well as forming homotetramers and homooctamers (Carr *et al.*, 1993; Colby *et al.*, 1999). Both isoforms have been reported to be present in RRs (Gunter *et al.*, 2008).

We quite unexpectedly found strong and specific staining of RRs by a number of monoclonal antibodies to the regulatory GTPase ARL2 (ARF-like 2; Clark *et al.*, 1993). ARL2 is an essential and very highly conserved GTPase within the ARF superfamily, predicted to have been present in the last eukaryotic common ancestor and ubiquitous in eukaryotes (Clark *et al.*, 1993; Li *et al.*, 2004; Klinger *et al.*, 2016). It localizes to several cellular locations including centrosomes (Zhou *et al.*, 2006), the nucleus (Muromoto *et al.*, 2008), and mitochondria (Newman *et al.*, 2014, 2017a,b), although the clear majority is found in cytosol, as part of a heterotrimeric complex with the tubulin cochaperone cofactor D and β-tubulin (Bhamidipati *et al.*, 2000; Francis, 2017a, 2017b). We have focused in recent years on defining the roles of ARL2 in tubulin biogenesis in cytosol (Francis *et al.*, 2017a,b) and both mitochondrial fusion (Newman *et al.*, 2017a,b) and ATP generation in mitochondria (Newman *et al.*, 2014), although it has also been linked to centrosome stability (Zhou *et al.*, 2006) and transport of N-myristoylated protein cargoes (Ismail *et al.*, 2011; Watzlich *et al.*, 2013).

Here we report a detailed characterization that extends our initial observation and leads us to the conclusion that RRs display much greater complexity in composition than suggested by the literature in this field. These results are likely to expand our understanding of the set of processes in which RRs are implicated.

RESULTS

RR size, shape, and quantity (both number per cell and prevalence within a cell population) are highly variable depending on the cell line under study. The manner and extent to which different cell types elaborate RRs in the absence of any inducer (normal cell culture conditions) or in response to different drug treatments and growth conditions, also varies. We carried out experiments using a variety of cell lines to test the generalizability of our results. With the exception of electron microscopy data, each experiment was typically repeated in at least three different cell lines; including some combination of HeLa, MEF (mouse embryo fibroblasts), NRK (normal rat kidney), IMCD3 (murine inner medullary collecting duct), human primary fibroblast, COS7 (African green monkey kidney), MDCK (Madin-Darby canine kidney), and NIH3T3 (mouse embryo fibroblast) cells. A summary of the results obtained in each is shown in Table 1. The results displayed are representative of all cell lines tested unless otherwise noted.

The regulatory GTPase ARL2 localizes to RRs

Upon characterization of a number of new monoclonal antibodies specific to ARL2, we found that ARL2 localizes to large cellular structures matching the appearance of RRs. To confirm the identity of these ARL2-positive structures, we compared the ARL2 staining to that of IMPDH2, a well-established marker of RRs (Ji *et al.*, 2006; Carcamo *et al.*, 2011; Juda *et al.*, 2014; Calise *et al.*, 2015). When costaining fixed cells with rabbit polyclonal antibodies directed against IMPDH2 and any of several mouse monoclonal antibodies raised against human ARL2, we observed very strong colocalization (Figure 1). Every ARL2-positive structure in every cell was IMPDH2-positive and vice versa, although the staining intensity of ARL2 varied across cell types. Three different monoclonal antibodies raised against bacterially expressed human ARL2 (3B4.B4, 15E11.B11, and 19F6.F11) yielded the same results. All of the ARL2 monoclonal staining displayed here was performed using the 3B4.B4 ARL2 mouse monoclonal antibody (mAb).

To further confirm the nature of the ARL2-positive structures as RRs, we treated cells with 1 μM MPA for 4 h. Following addition of MPA, the size and quantity of ARL2-positive structures increased dramatically such that they were present in every cell, even in cell lines that display none of these structures under normal culture conditions, such as HeLa cells (Figure 1). The most intense ARL2 staining was observed in MPA-treated HeLa cells, while the weakest (but still readily observable) was seen in MEFs (Figure 1). ARL2 colocalization with IMPDH2 at RR-shaped structures was observed in all cell lines tested, at endogenous structures (structures present under normal growth conditions), and under all induction conditions. ARL2 staining intensity is consistent regardless of the induction method; however, the appearance of ARL2 at RRs can vary depending on the cell line. These variations are summarized in Table 1. Additionally, RRs localized within the nucleus have been previously reported (Calise *et al.*, 2014; Juda *et al.*, 2014). We found that ARL2 localizes to both cytoplasmic and nuclear RRs (Supplemental Figure S1), although ARL2 staining at nuclear RRs is sometimes difficult to discern due to ARL2 staining throughout the nucleus and the fact that nuclear RRs are typically shorter and finer than those observed in the cytosol. Thus, we conclude that ARL2 localizes to RRs based on its consistent colocalization with IMPDH2-positive and MPA-inducible structures in multiple cell types.

To confirm the specificity of both IMPDH2 and ARL2 antibody staining at RRs we carried out antigen competition using purified proteins. Prior incubation of the IMPDH2 antibody with purified, recombinant, human IMPDH2, followed by immunofluorescence staining of fixed cells resulted in near complete loss of IMPDH2 signal intensity at RRs compared with controls (Supplemental Figure S2). Similarly, prior incubation of the ARL2 mAb with purified ARL2

Conditions and antigens tested	Cell lines									Relevant literature
	HeLa	MEF	NRK	IMCD3	hFB	hFB-LND	MDCK	NIH3T3	COS7	
RRs present without inducers	–	+	+	+++	–	–	+++	+	–	Willingham *et al.* (1987), Gunter *et al.* (2008), Ramer *et al.* (2010), Carcamo *et al.* (2011), and Chang *et al.* (2015)
RRs induced by:										
MPA	+++	+++	++	+++	++	++	ND	ND	+	Ji *et al.* (2006), Gunter *et al.* (2008), Thomas *et al.* (2012), Calise *et al.* (2014, 2016), Chang *et al.* (2015), and Keppeke *et al.* (2015a, 2016)
Glucose starvation	–	+++	+	++	–	–	++	+	–	Noree *et al.* (2010)
AICAR	++	++	+++	+++	++	++	ND	ND	ND	
DON	+++	+++	++	++	++	++	ND	ND	ND	Carcamo *et al.* (2011), Calise *et al.* (2014), Chang *et al.* (2015), and Keppeke *et al.* (2015a,b)
Guanosine reversal	+++	+++	ND	+++	+++	–	ND	ND	ND	Gunter *et al.* (2008), Calise *et al.* (2014, 2016), and Keppeke *et al.* (2015b)
Colocalization at RRs										
ARL2 (MPA)	+++	+	++	++	+++	+++	++	+	+++	
ELMOD2 (glucose starvation)	+	++	+	+	ND	ND	+	+	ND	
Cofactor D (MPA)	–	+	+	+	ND	ND	ND	ND	ND	
Calnexin (glucose starvation)	+	++	++	++	ND	ND	ND	ND	ND	
GRP78 (glucose starvation)	ND	++	ND	+	ND	ND	ND	ND	ND	
SigmaR1 (glucose starvation)	ND	++	ND	+	ND	ND	ND	ND	ND	
Sec61β (glucose starvation)	ND	ND	ND	+	ND	ND	ND	ND	ND	
CTPS1 (DON)	–	ND	+/–	+/–	ND	ND	ND	ND	ND	Carcamo *et al.* (2011), Chang *et al.* (2015), and Keppeke *et al.* (2015b)

Conditions of cell culture or the antibodies used in double labeling are shown on the left. Cell lines are listed along the top. A plus (+) indicates the presence of RRs or colocalization at RRs, additional plus signs (+++) indicates a stronger signal than seen in other cells, and a minus sign (–) indicates the absence of RRs or of colocalization at RRs. For RR colocalization, the inducer that leads to the strongest staining intensity is indicated in parentheses. ND = not done. Citations to relevant literature are included in the rightmost column.

TABLE 1: Summary of results from multiple different cell lines and their responses to different inducers of RRs, reversal by guanosine, and colocalization of different antigens with IMPDH2 or ARL2.

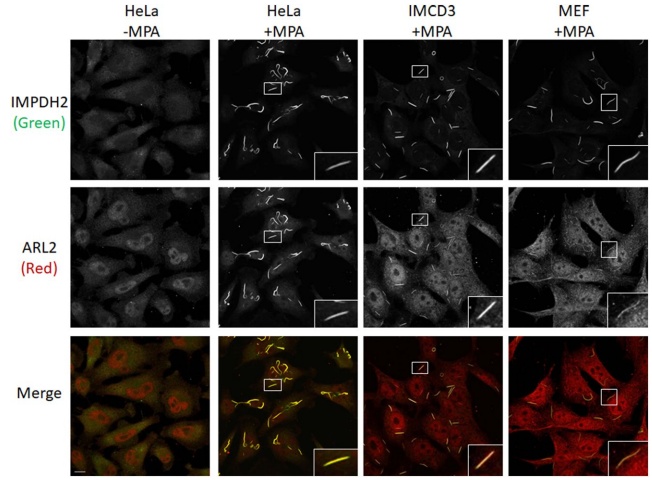

FIGURE 1: ARL2 localizes to IMPDH2-positive structures that are inducible with MPA. HeLa (first two columns), IMCD3 (third column), and MEF (last column) cell lines were treated with either vehicle control (–MPA) or 1 μM MPA (+MPA) for 4 h. Cells were then fixed and costained for IMPDH2 (top row) and ARL2 (middle row), as described under *Materials and Methods*. Two-dimensional (2D) projections of Z-stacks are shown. Scale bar in bottom left panel = 10 μm and is the same for each image. Insets show zoomed-in versions of individual rods.

protein led to a corresponding decrease in ARL2 signal at RRs when the antibody was then used for immunofluorescence (Supplemental Figure S2). This further confirms the specificity of the IMPDH2 and ARL2 signals we observe at RRs using our rabbit polyclonal IMPDH2 and mouse monoclonal ARL2 antibodies.

We also performed double labeling with mouse monoclonal and rabbit polyclonal antibodies, each directed against ARL2, and found complete overlap in staining at RRs, although less so at other structures (Supplemental Figure S3). Indeed, our ARL2 monoclonal antibodies robustly stain RRs but react much more weakly than the polyclonal serum with cytosolic and mitochondrial ARL2 (Supplemental Figure S3). This makes our ARL2 monoclonal antibodies quite useful for visualization of RRs as they display a clear preference for staining RRs over other structures. Reasons for this preferential staining of different structures between the antibodies are not understood, but the availability of both rabbit and mouse antibodies allowed us to perform double labeling with antibodies directed against many other antigens.

AICAR induces RR formation

To date, RR induction has been most commonly observed upon treatment of cells with drugs that either directly or indirectly inhibit IMPDH, for example, MPA that traps a covalent intermediate of IMPDH with covalently bound nucleotide and inhibits this key step in guanine nucleotide biosynthesis. Before we identified the ARL2-positive structures as RRs, we suspected the structures may be related to macroautophagy. To test this, we treated cells with 5-aminoimidazole-4-carboxamide ribonucleotide (AICAR) to promote autophagy via activation of AMP kinase (AMPK). Interestingly, we found that AICAR robustly induces the formation of RRs (Figure 2). AICAR is also an intermediate in the IMP pathway. It is the substrate for the enzyme just upstream of IMPDH, although it has not previously been reported to cause RR formation. All cells displayed at least one RR structure within 2 h of AICAR treatment. RRs remained present in all AICAR-treated cells for at least 24 h. However, the size

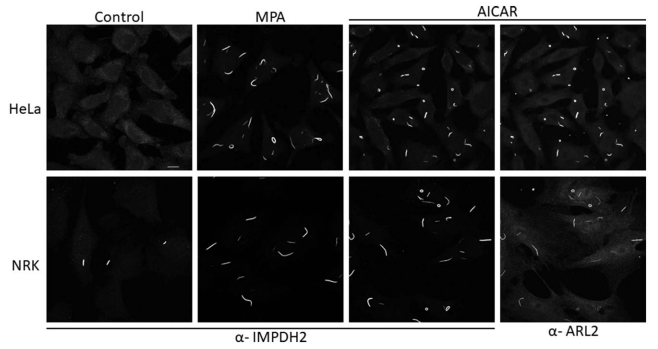

FIGURE 2: AICAR induces RR formation. HeLa (top row) or NRK (bottom row) cells were treated with either vehicle control (leftmost column), 1 μM MPA (second column), or 1 mM AICAR (right two columns) for 2 h. Cells were then fixed and costained for IMPDH2 and ARL2. Only the IMPDH2 staining is shown in the two leftmost columns, while both IMPDH2 (third column) and ARL2 (fourth column) costaining are shown on the two columns to the right. 2D projections of Z-stacks are shown. Scale bar = 10 μm.

of RRs differs when comparing AICAR- to MPA-treated cells, regardless of treatment time. With the exception of NRK cells, RRs induced by AICAR were smaller than those formed by MPA induction, although they are still larger than RRs observed in uninduced cells (Figure 2). In contrast to other cell types, in NRK cells, RRs induced by either AICAR or MPA were similar in size. NRK cells are also unusual in having almost no rings at all after treatment with MPA (Figure 2). Like with MPA treatment, AICAR-induced RRs were always found to stain positively for both IMPDH2 and ARL2 (Figure 2).

As previously mentioned, AICAR is also a well-known activator of AMPK (Russell *et al.*, 1999). To test whether the induction of RRs with AICAR is a result of AMPK activation, we treated AMPK-null MEFs (MEFs lacking *ampk1* and *ampk2* [Laderoute *et al.*, 2006]) with AICAR and compared RR induction to paired control MEFs. In both, AICAR was capable of dramatic RR induction (Figure 3), suggesting that RR induction with AICAR was independent of AMPK activation.

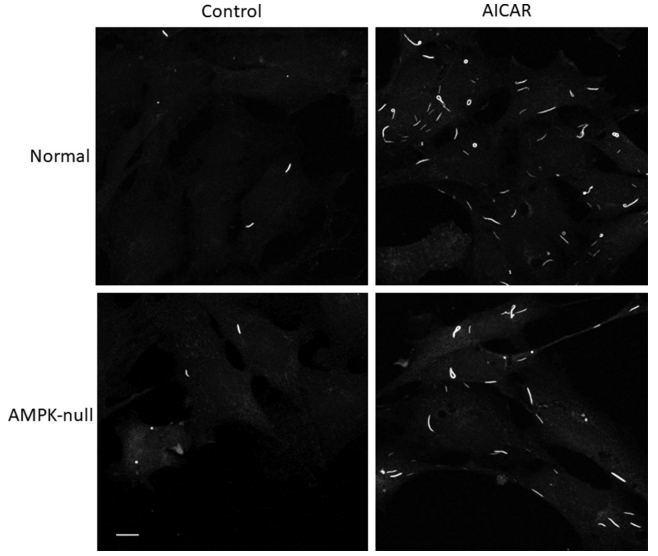

FIGURE 3: AICAR is capable of inducing RR formation in AMPK–null MEFs. AMPK–null MEFs (bottom) and paired control MEFs (top) were treated with vehicle control (left) or 1 mM AICAR (right) for 2 h. Cells were then fixed and stained for IMPDH2. 2D projections of Z-stacks are shown. Scale bar = 10 μm.

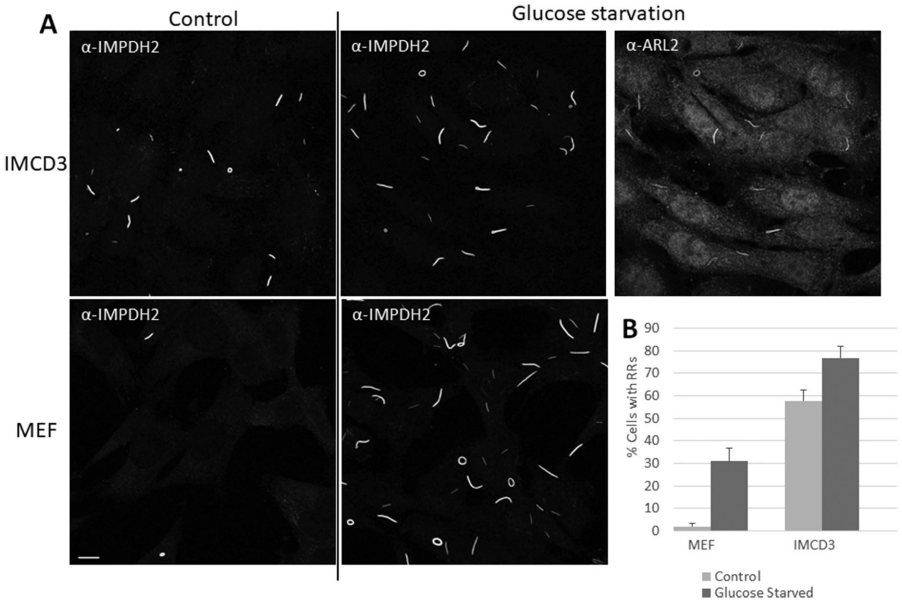

FIGURE 4: Glucose starvation increases the percentage of cells with RRs. (A) IMCD3 (top row) or MEF (bottom row) cell lines were grown in either normal medium (left) or glucose-free medium (middle) for 24 h. Cells were then fixed and costained for IMPDH2 (left and middle) and ARL2 (right). 2D projections of Z-stacks are shown. Scale bar = 10 μm. (B) Cells treated as described in A were scored for the presence of RRs. The percentage of cells with at least one RR is shown. *N* = 200 for each cell line and condition. Scale bars represent SD of two independent experiments.

Additionally, A-769662, another activator of AMPK (Liu *et al.*, 2016), had no impact on RR size or quantity. Thus, it is likely that increasing AICAR levels act by altering the pools of one or more intermediates or products of the de novo and guanine nucleotide biosynthetic pathways which leads to RR formation.

Glucose starvation also induces RR formation

We recently showed that glucose starvation (cell culture in medium lacking glucose for up to 48 h) caused changes in the staining intensity of ARL2 in mitochondria (Newman *et al.*, 2017b). Using the same regimen, we found that glucose starvation also increases the percentage of cells with RRs that stain positively for both IMPDH2 and ARL2 (Figure 4). Unlike MPA or AICAR, glucose starvation does not cause as robust an increase in the percentage of cells with RRs (Figure 4B). The proportion of cells which form RRs in response to glucose starvation varies greatly depending on the cell line. IMCD3 (Figure 4B), NRK, MDCK, and NIH3T3 show a moderate increase in the percentage of cells with at least one RR, compared with control conditions, while the fold increase is more dramatic in MEFs (Figure 4B). Several other cell lines (HeLa, COS7, G361, human fibroblasts) do not form RRs in response to glucose starvation. Notably, these are the same cell lines in which we have never observed RRs under normal growth conditions. In the rest of the cell lines tested, RRs can be observed in at least a small percentage of cells under normal growth conditions. In cell lines where glucose starvation has a strong effect on RR quantity, the fraction of cells with at least one RR never reaches 100% (e.g., IMCD3 cells peak at ~75% [Figure 4B]).

RRs were also slower to form after switching to the no glucose medium, compared with drug treatments. Whereas 2 h was sufficient for 100% of cells to display RRs following MPA or AICAR addition, an increase in RR quantity following glucose starvation was not evident until at least 6 h after glucose removal and did not peak until 24 h. In almost all cell lines in which glucose starvation induced RRs, we observed an increase in their number, but not size. MEFs were an exception, as glucose starvation increased both the quantity and size of RRs in this line, although they were still not as large as the RRs observed in MPA-treated MEFs.

The induction of RRs did not seem to be a generalized response to cell stress or growth inhibition. We tested a number of other drugs (3-methyladenine, bafilomycin, 2-deoxy glucose, metformin, oligomycin, antimycin A, cycloheximide, compound C, nocodazole, latrunculin A), as well as serum starvation, none of which influenced the size or quantity of RRs.

Guanosine fails to prevent RR formation in fibroblasts from Lesch–Nyhan disease patients

RR formation has been linked to guanine nucleotide metabolism in large part because the marker of RRs, IMPDH, is the rate-limiting step in de novo synthesis of guanine nucleotides, and inhibitors of the enzyme are strong inducers of RRs. There also exists a salvage pathway in which guanine or guanosine can be imported from outside the cell and converted directly to GMP. Addition of guanosine has been shown to prevent or reverse the formation of constitutive or MPA-induced RRs (Calise *et al.*, 2014, 2016). We recapitulated these findings in multiple cell lines (Supplemental Figure S4). It has been suggested that guanosine feeds into the salvage pathway for guanine nucleotide production, compensating for the inhibition of the de novo pathway that results when cells are treated with IMPDH inhibitors. If so, this pathway would be diminished or lost in cells which have mutated hypoxanthine-guanine phosphoribosyltransferase (HGprt), the enzyme needed to convert guanine into GMP. Human cells with such mutations are available from patients with Lesch–Nyhan disease (LND; Fu *et al.*, 2015). Guanosine is normally converted first to guanine by purine nucleoside phosphorylase and then recycled into GMP by HGprt. Thus, if added guanosine prevents RR formation because of its ability to restore guanine nucleotides, we would predict that guanosine addition would have no such effect in LND fibroblasts, where guanosine incorporation into guanine nucleotides is defective.

Both normal and LND fibroblasts showed no RRs under control conditions and a robust induction of RRs following MPA treatment (Figure 5). Addition of 1 mM guanosine with MPA (1 μM) completely prevented RR formation in control human fibroblasts. However, when the same treatment was applied to LND fibroblasts, all cells formed obvious RRs, appearing identical to the MPA-only condition (Figure 5). This result suggests that it is not guanosine, but rather guanine nucleotides, which reverse RR formation following MPA.

It has been previously reported that interfering with de novo synthesis of guanine nucleotides by glutamine starvation or inhibition of dihydrofolate reductase, will induce the formation of RRs and that the addition of guanosine completely reverses this effect (Calise *et al.*, 2014, 2016). We found that guanosine is also capable of reversing RRs formed via AICAR treatment or glucose starvation (Supplemental Figure S5). These results support the hypothesis that RR formation is closely linked to guanine nucleotide pools regardless of

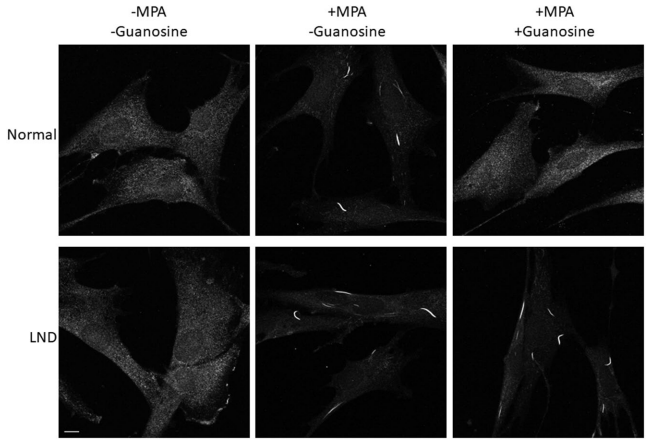

FIGURE 5: Guanosine does not prevent RR formation in LND fibroblasts. Normal human fibroblasts (top) and fibroblasts derived from patients with LND (bottom) were treated with vehicle control (left), 1 μM MPA (middle), or 1 μM MPA + 1 mM guanosine (right) for 4 h. Cells were then fixed and stained for IMPDH2. 2D projections of Z-stacks are shown. Scale bar = 10 μm.

induction methods, and that guanosine is able to prevent or reverse RR formation by generating guanine nucleotides via the purine salvage pathway.

ARL2 always colocalizes with IMPDH2 at RRs but not with CTPS1 at cytoophidia

Cytoophidia are similar to RRs in being large structures that form in response to glutamine analogues such as DON or acivicin (Carcamo *et al.*, 2011; Calise *et al.*, 2014; Keppeke, *et al.*, 2015a). These drugs inhibit a range of enzymes which bind glutamine, including CTPS (Pinkus, 1977). Although there are several similarities between RRs and cytoophidia, there are also important differences. MPA never induced the formation of CTPS1-positive cytoophidia in HeLa cells and only rarely (~10% of cells) did so in NRK or IMCD3 cells (Figure 6). Unlike RRs, we never observed any cytoophidia under normal growth conditions in any of the cell lines tested and neither AICAR nor glucose starvation induced the formation of cytoophidia.

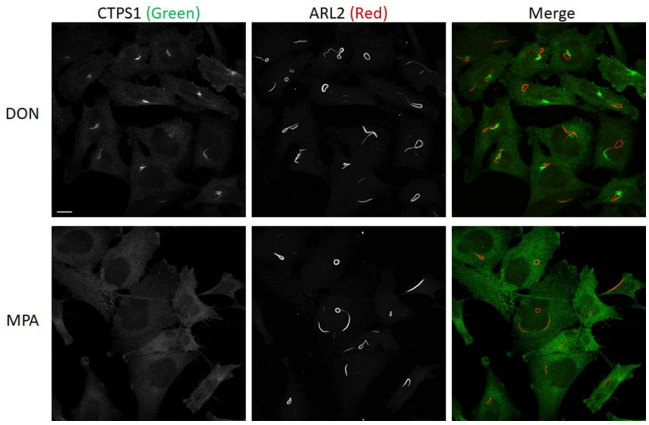

FIGURE 6: ARL2 does not localize to CTPS1-positive structures that are induced with DON but does colocalize with IMPDH2-positive RRs. HeLa cells were treated with either 100 μM DON (top) or 1 μM MPA (bottom) for 24 h. Cells were then fixed and costained for CTPS1 (left) and ARL2 (middle). 2D projections of Z-stacks are shown. Scale bar = 10 μm.

ARL2 only rarely colocalized with CTPS1. In NRK and IMCD3 cells, ARL2 and CTPS1 antibodies sometimes costained what appears to be the same rod-like structures, but in the same cell or others in the culture there were also many more structures positive for ARL2 or CTPS1, but negative for the other. HeLa cells serve as a striking example in which ARL2 and CTPS1-positive structures were often in close proximity but did not colocalize (Figure 6). This is in stark contrast to the consistent colocalization between ARL2 and IMPDH2 (Figure 1). The shape of cytoophidia was also obviously different compared with RRs in HeLa cells with cytoophidia being shorter, thicker, and lacking rings (Figure 6). We conclude that although RRs and cytoophidia often displayed a physical proximity, suggesting they may sometimes share an underlying substructure, they were clearly distinct structures and that ARL2 is a component of RRs but not cytoophidia.

A specific subset of ARL2 partners localize to RRs

We examined whether other members of the ARF family localized to RRs. Immunofluorescence using a rabbit polyclonal antibody directed against ARL3, the closest paralogue of ARL2 sharing 53% identity (Li *et al.*, 2004; Logsdon and Kahn, 2004), displayed localization to centrosomes as previously described (Zhou *et al.*, 2006) but no colocalization at RRs in any of the cell lines tested (Supplemental Figure S6). In agreement with those stark differences in immunolocalization results, we saw no evidence of cross reactivity in immunoblots when ARL2 and ARL3 antisera were used to probe the purified recombinant GTPases. Other members of the ARF family tested include ARL1, ARL13b, ARF1, ARF3, ARF4, and ARF6. None of these localized to RRs.

We next asked whether known ARL2 binding partners were also present at RRs. We had earlier purified ELMOD2 from mammalian tissues as an ARL2 GTPase-activating protein (GAP) and later showed that it is one of a three-member family of paralogues in mammals, ELMOD1-3 (Bowzard *et al.*, 2007; East *et al.*, 2012). The ELMOD (cell EnguLfment and MOtility Domain) proteins each share a single (ELMO) domain with the three ELMO proteins in mammals (Chung *et al.*, 2000; Gumienny *et al.*, 2001), yet appear to have quite distinct functions, with only the ELMODs acting as GAPs for ARF family GTPases (Bowzard *et al.*, 2007; East *et al.*, 2012; Ivanova *et al.*, 2014). Double labeling for ELMOD2 and ARL2 revealed clear colocalization at RRs (Figure 7A). This was evident in all cells examined, although less obviously so in HeLa cells. The staining of ELMOD2 at mitochondria and other sites made its presence at RRs less obvious compared with the ARL2 monoclonal antibodies, but every ARL2-positive RR (both endogenous and following induction) also stained positively for ELMOD2. The staining intensity of ELMOD2 at RRs was more intense following AICAR or glucose-starvation induction compared with MPA induction. In marked contrast, other members of the ELMOD family (ELMOD1 and ELMOD3) did not localize to RRs under any of these conditions (Supplemental Figure S6).

We also observed that cofactor D colocalized with ARL2 at RRs (Figure 7B). Cofactor D exists in a 1:1:1 complex with ARL2 and β-tubulin and is one of several cofactors involved in αβ-tubulin biogenesis (Tian *et al.*, 1996; Shern *et al.*, 2003; Francis *et al.*, 2017b). The other tubulin cofactors (cofactors A, B, C, and E) showed no evidence of staining at RRs (Supplemental Figure S6). Like ELMOD2, cofactor D colocalization at RRs was observable in all cell lines tested with the exception of HeLa. Cofactor D staining was observable at RRs under control and all induction conditions with no obvious differences in staining intensity between the induction methods. Cytosolic cofactor D staining sometimes impedes visualization of

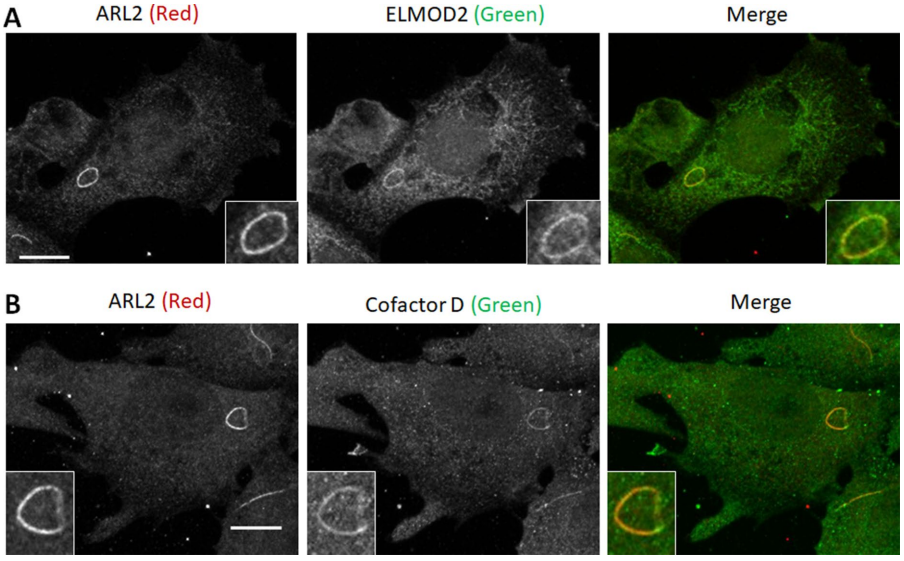

FIGURE 7: A subset of ARL2 binding partners localize to RRs. (A) MEFs were grown under glucose-starvation conditions for 48 h and then fixed and costained for ARL2 (left) and ELMOD2 (middle). (B) MEFs were treated with 1 μM MPA for 2 h and then fixed and costained for ARL2 (left) and cofactor D (middle). In each case, 2D projections of Z-stacks are shown. Scale bar = 10 μm. Insets show zoomed-in versions of individual rings.

The ratio of rods to rings varies between cell types, although rods always outnumber rings. Rings are easier to identify as RRs because, although rods might be mistaken for cilia or mitochondria, rings of this size are highly unusual in cells. For this reason, our figures more often show rings, even though they are fewer in number. We found no antibody that exhibited a clear preference in staining rods over rings or vice versa.

Binder of ARL2 (BART aka ARL2BP) was the first ARL2 partner identified, based on its specific interaction with activated, GTP-bound ARL2 (Sharer and Kahn, 1999; Sharer *et al.*, 2002; Bailey *et al.*, 2009; Zhang *et al.*, 2009). Like ARL2, BART is found predominantly in cytosol but also localizes to mitochondria (Sharer *et al.*, 2002). Our rabbit polyclonal antibodies to BART found no evidence of staining of RRs. Thus, overall, these data demonstrate that there is a specific set of ARL2 binding partners, including ELMOD2 and cofactor D, that colocalized with ARL2 and IMPDH2 to RRs, whereas others, ELMOD1/3, BART, and cofactors A/B/C/E, did not.

cofactor D at RRs, although not to the same extent as ELMOD2. This may be because cofactor D staining usually appeared diffuse (as opposed to ELMOD2 which appeared punctate/mitochondrial), making the RR structures more easily discernible. β-tubulin did not localize to RRs by immunofluorescence, although we cannot exclude the possibility that some β-tubulin was present but key epitopes are masked in the trimer.

RRs are associated with an ER-derived membrane

The localization of ARL2, cofactor D, and ELMOD2 to RRs suggests that RRs are more complex than simple polymers of IMPDH. We examined the localization of well-established markers of various cellular organelles and found that several resident ER proteins colocalized with ARL2 at RRs. The most striking colocalization was observed with calnexin (Figure 8A), a transmembrane, resident ER protein which can escape and be found at the cell surface (Wiest *et al.*, 1995, 1997; Charonis *et al.*, 2017). The next most prominent RR staining of a resident ER protein was another lumenal chaperone GRP78 (Figure 8B), which also can escape to the plasma membrane (Tsai *et al.*, 2018). Although its staining of RRs was comparable to that of calnexin, there was additional cytoplasmic staining that made RR staining with GRP78 antibodies less prominent. This was also seen for SigmaR1 (Figure 8C), another transmembrane, ER-resident protein that is thought to accumulate in lipid rafts and at ER–mitochondria contact sites (Ruscher and Wieloch, 2015).

In contrast to the immunofluorescence localization of *endogenous* proteins described so far, we used exogenous expression of mCherry-tagged Sec61β due to the lack of an antibody capable of specifically staining the endogenous protein. mCherry-Sec61β also colocalized with RRs (Supplemental Figure S7). Each of these proteins contains a transmembrane domain with the exception of GRP78 which resides in the ER lumen (Bole *et al.*, 1986). The colocalization of these ER proteins at RRs was consistently observed in multiple cell lines, except for mCherry-Sec61β, which had the weakest colocalization and was observed only in IMCD3 cells.

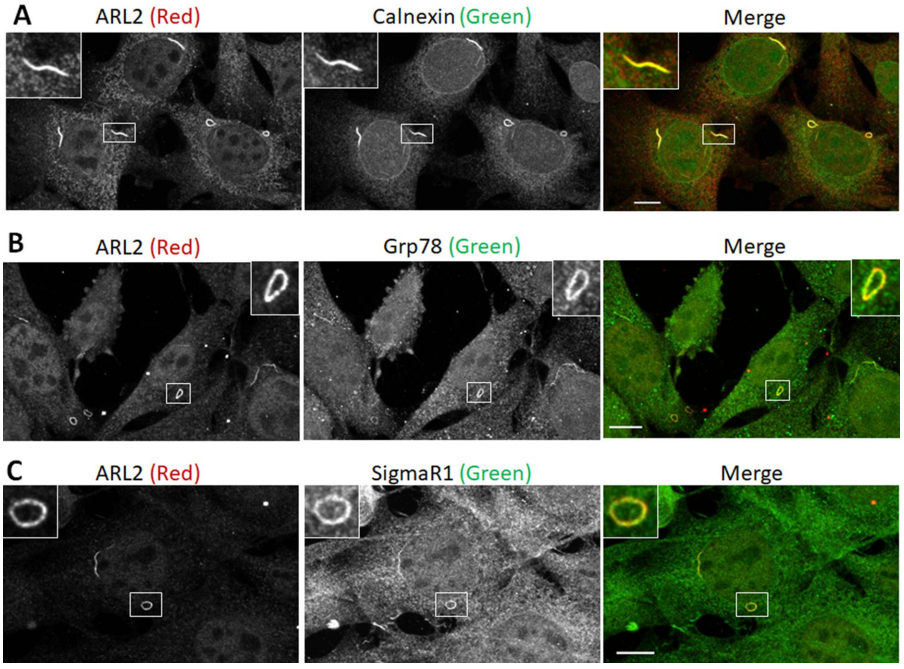

FIGURE 8: Three different ER membrane proteins also colocalize with RRs. MEFs were grown under glucose-starvation conditions for 24 h and then fixed and costained for ARL2 (left) and (A) calnexin (top middle), (B) GRP78 (middle), or (C) SigmaR1 (bottom middle). 2D projections of Z-stacks are shown. Scale bar = 10 μm. Insets show zoomed-in versions of individual rods for A and rings for B and C.

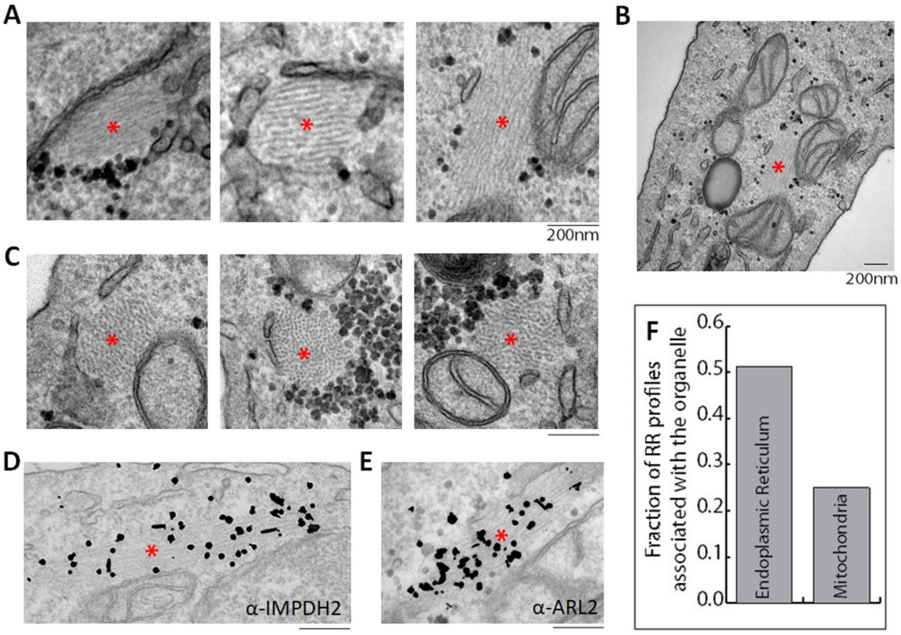

FIGURE 9: The filamentous nature of RRs is evident by EM staining and ARL2 and IMPDH2 colocalize to RRs as seen by immunogold staining. HeLa cells were induced with 1 μM MPA for 2 h and processed for EM, as described under *Materials and Methods*. All scale bars = 200 nm. (A) Longitudinal sections of RRs. The RRs are indicated by an asterisk (*). (B) A zoomed-out image of the RR shown in the far-right image from A. (C) Transverse sections of RRs. Labeling scheme is the same as A. (D) Immuno-EM showing localization of IMPDH2 using IMPDH2 antibody coupled to nanogold particles. The asterisk marks the RR while the black particles indicate the IMPDH2 localization. (E) Same as D except using ARL2 antibody to show localization of ARL2. (F) The fraction of RRs that were associated with the ER or mitochondrial membranes were counted in randomly acquired EM images of the RRs and plotted. $N = 45$.

Colocalization of ER proteins at RRs was tested under control, glucose-starvation, and MPA-treatment conditions. Although colocalization between the previously listed ER proteins and RRs was observable under all of these conditions, the staining intensity was highest after glucose starvation (with the exception of cells in which glucose starvation does not induce RRs; Supplemental Figure S8).

In contrast to calnexin, GRP78, and SigmaR1, at least one other ER protein, calreticulin, did not localize to RRs (Supplemental Figure S9). This finding raises the possibility that a subcompartment of the ER associates with RRs. Other organelle markers that we tested included TGN46 (Golgi), HSP60 (mitochondria), α- and β-tubulin (microtubules), rhodamine phalloidin (actin), acetylated tubulin (primary cilia), and LC3 (autophagosomes)—none of which was observed at RRs (Supplemental Figure S9). The presence of multiple transmembrane ER proteins at RRs suggests that the ER, or a membrane derived from the ER, is closely associated with RRs.

Ultrastructural data support the presence of ARL2 throughout RRs and association of RRs with a membrane

To further explore the association of both ARL2 and a membrane with RRs, we used transmission electron microscopy (EM) to visualize RRs in HeLa cells treated with MPA (1 μM) for 2 h. As seen previously (Juda *et al.*, 2014), RRs appeared as a collection of long, clustered filaments in longitudinal sections and as a bundle of filaments in cross-section (Figure 9, A and C, respectively). Using nanogold labeling with silver enhancement, in conjunction with the polyclonal IMPDH2 antibody, we observed localization of IMPDH2 throughout the RRs, as expected (Figure 9D). Immunolabeling throughout RRs was equally evident upon staining with a monoclonal ARL2 antibody, consistent with our immunofluorescence data (Figure 9E). It was also common to observe clusters of darkly staining glycogen granules adjacent to RRs (Figure 9), although we did not further explore this observation.

Intracellular membranes were often found to be in close apposition to rods by EM (Figure 9). These membranes appeared to be ER and mitochondria, based on their morphologies; however, the membrane typically did not run along the entire length of the rod (Figure 9B). We quantified the fraction of RRs with closely apposed membranes and found about half to lie along the ER and about a quarter were adjacent to a mitochondrion (Figure 9F).

Different components of RRs have different kinetics of recruitment

We sought to monitor the assembly of RRs over time, to establish whether it is an ordered process. We compared the kinetics of RR formation in three cell lines after addition of MPA (1 μM) over a 2 h window, by costaining for IMPDH2 and ARL2 (Figure 10). The formation of RRs was quite consistent across cell lines, with MEFs progressing slightly faster than HeLa or NRK cells, but all three reaching their peak of 100% of cells with RRs within 1–2 h after MPA addition (Figure 10, A and B). Within 5 min of MPA treatment, IMPDH2-positive structures were observed in a small percentage of cells (Figure 10A). At this time they were dispersed throughout the cytosol, appearing to have a punctate morphology, and were far more numerous and much smaller in size than mature RRs. The same was true in MEFs and NRK cells except the morphology appeared less punctate and more like small, extremely thin rods. The size and number of RRs per cell changed over time, with the number of structures per cell decreasing and the size and thickness of the structures increasing (Figure 10A). Visual inspection of such time course data also suggests that IMPDH2 staining was more diffuse before, or at early time points after, MPA addition, consistent with the mass movement of IMPDH2 from the soluble fraction into RRs. Such a change in localization is suggestive of the lack of need for new protein synthesis, although not formally tested here.

ARL2 appears to recruit to RRs after IMPDH2. Costaining of ARL2 and IMPDH2 over time revealed that ARL2 was not recruited to RRs until ~20 min after MPA addition, while IMPDH2-positive structures were evident at 5 and 10 min (Figure 10, A and C). The accumulation of ARL2 at RRs appears to coincide with the change in RR morphology from a punctate (or very thin rod) shape to the more typical RR shape; that is, ARL2 colocalization is rarely visible at punctate structures but almost always visible at RR-shaped structures. This difference between IMPDH2 and ARL2 staining and the change in morphology were most dramatic between 10 and 20 min. At later times the two proteins stained indistinguishably.

In contrast to IMPDH2 or ARL2, calnexin recruitment to RRs was slower and only ~40% of cells showed calnexin at RRs after 45 min in MPA, at which point ARL2 was seen at RR in more than 80% of

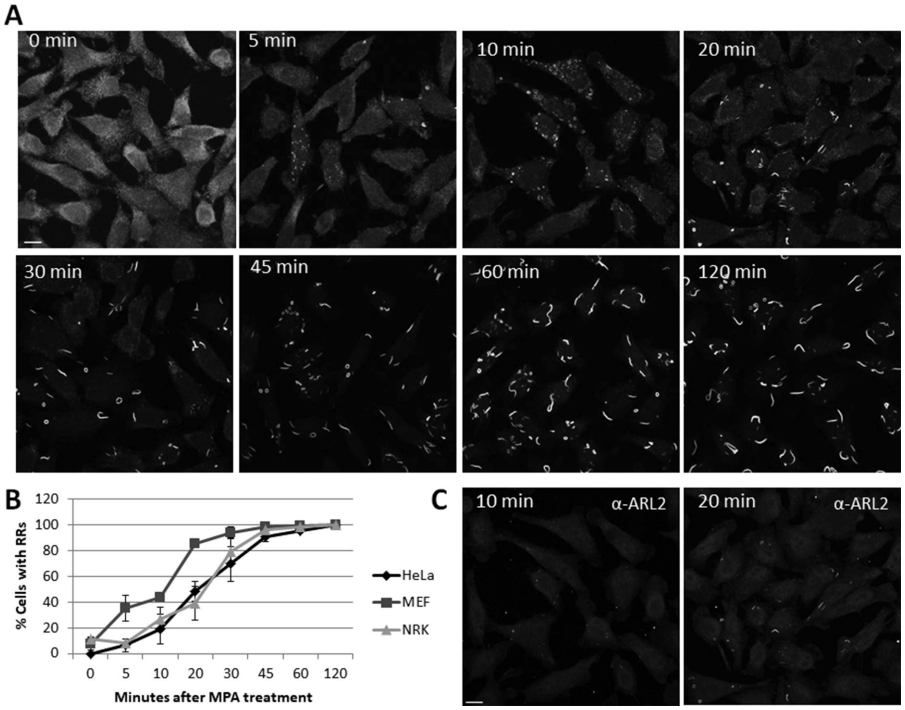

FIGURE 10: RRs increase in size and quantity over time after induction with MPA. HeLa, MEF, or NRK cells (HeLa cells are pictured) were fixed at the times shown after addition of MPA (1 μM). Cells were then costained for IMPDH2 and ARL2. (A) IMPDH2 staining is shown. Images were collected and processed identically at every step for each time point. 2D projections of Z-stacks are shown. Scale bar = 10 μm. (B) Cells treated as described in A were scored for the presence of RRs based on IMPDH2 staining. The percentage of cells with at least one RR is shown. *N* = 100 for each time point and cell line. Error bars represent SD between two independent experiments. (C) ARL2 staining is shown at the 10 and 20 min time points (same fields shown in panel A). 2D projections of Z-stacks are shown. Scale bar = 10 μm.

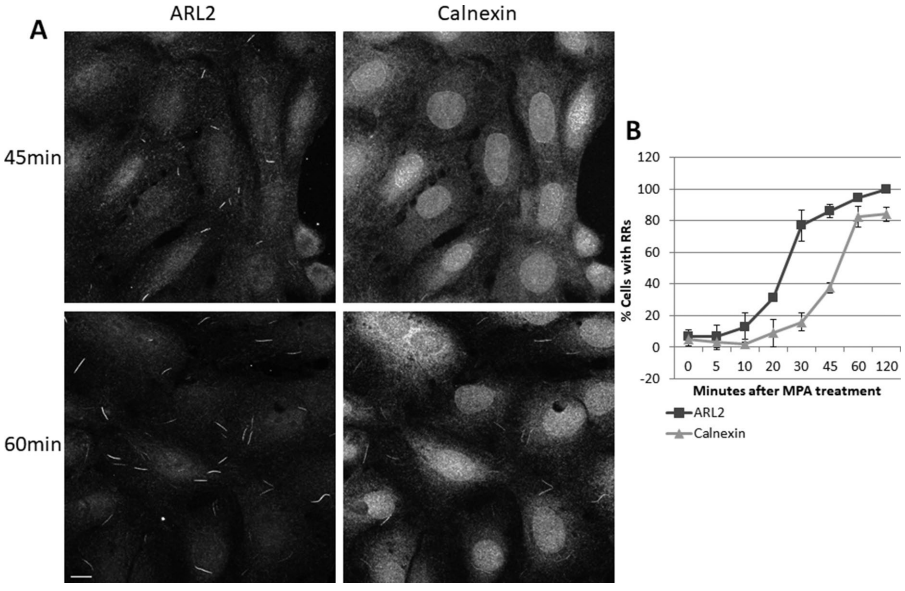

FIGURE 11: Calnexin recruits to RRs well after IMPDH2 and ARL2. (A) HeLa, MEF, or NRK cells (NRK cells are pictured) were fixed at different times after addition of MPA (1 μM). Cells were then costained for ARL2 and calnexin, as described under *Materials and Methods*. ARL2 (left) and calnexin (right) at 45 min (top) and 60 min (bottom) are shown. 2D projections of Z-stacks are shown. Scale bar = 10 μm. (B) NRK cells treated as described in A were scored for the presence of RRs based on ARL2 or calnexin staining. The percentage of cells with at least one RR is shown. *N* = 100 for each time point. Error bars represent SD between two independent experiments.

cells (Figure 11). Thus, these time course data are consistent with an ordered and sequential addition of components, with IMPDH the first protein to polymerize, ARL2 arriving slightly later, and calnexin recruitment still later.

DISCUSSION

We provide evidence that a number of proteins not directly involved in nucleotide metabolism are present at RRs. They appear to be recruited to RRs with a high degree of specificity and in an ordered manner, consistent with them playing specific roles. We demonstrate that the regulatory GTPase ARL2 is a component of RRs, based on its colocalization with IMPDH2 in every cell line tested and the coordinated increases in each upon treatment with each of the inducers of RR formation, most notably MPA (Figure 1). We also describe for the first time two treatments that promote RR formation, AICAR and glucose deprivation, which also contain ARL2. Among the other newly identified proteins found to colocalize at RRs are a number of ER proteins, leading us to propose a role for the ER in RR biology. These newly discovered components of RRs and means of induction also allow us to draw clear distinctions between RRs and cytoophidia.

The localization of ARL2 to RRs was observed in every cell line tested, although with variability in the staining intensity (Table 1). ARL2 localization was also evident at the EM level, in which ARL2 could be seen throughout the RRs (Figure 9). In contrast, other members of the ARF family, including the closest paralogue to ARL2, ARL3, were not found at RRs (Supplemental Figure S5). Specificity was also evident in the ARL2 interacting partners present in RRs, ELMOD2 and cofactor D (Figure 7), as others were not found there (ELMOD1, ELMOD3, BART, other tubulin cofactors). We have focused in recent years on defining the roles of ARL2 in tubulin biogenesis (Francis *et al.*, 2017a,b), mitochondrial fusion (Newman *et al.*, 2017a,b), and ATP generation in mitochondria (Newman *et al.*, 2014). ELMOD2 appears to work together with ARL2 in the mitochondrial intermembrane space to affect fusion. ARL2 function has also been linked to centrosome stability (Zhou *et al.*, 2006) and transport of N-myristoylated protein cargoes (Ismail *et al.*, 2011; Watzlich *et al.*, 2013). Given this diversity of ARL2 actions, there are several potential functional links to RRs to be examined. It is also possible that inclusion of ARL2 (and cofactor D/ELMOD2) in RRs may serve to sequester it away from other sites and actions, in what has been termed "higher order signaling" (Francis *et al.*, 2016).

Surprisingly, a number of ER-resident, membrane proteins were also found associated with RRs (Figure 8). The costaining of IMPDH2 with these ER proteins leads us to propose a role for the ER, or a subcompartment derived from it, in RR biology. We found that calnexin, GRP78, SigmaR1, and Sec61β all colocalize with IMPDH2 at RRs (Figure 8). With the exception of GRP78, each is a transmembrane protein, so their localization to RRs strongly implies that there is a membrane component associating with RRs. Because calreticulin, another common ER marker, does not colocalize with RRs we speculate that only a subcompartment of the ER interacts with RRs. Previous reports have not found RRs associated with membrane when visualized using EM (Ji *et al.*, 2006; Thomas *et al.*, 2012; Juda *et al.*, 2014), and we too find examples of RR that are not proximal to a membrane. Although the membrane proteins (e.g., calnexin) appear to colocalize along the entire length of RRs when visualized by immunofluorescence, this is not the case for membranes seen in our EM images. We cannot currently explain this apparent difference, although they may arise during sample preparation required by the different techniques of staining. It is also possible that these differences are amplified by using MPA to induce the RRs observed by EM as the staining intensity of ER-associated proteins is more intense in RRs induced by glucose starvation (Supplemental Figure S8). This was also true of ELMOD2, which has been reported to partially localize to the ER (Suzuki *et al.*, 2015). On the other hand, IMPDH2, ARL2, and cofactor D (all primarily cytosolic proteins) showed no such difference in staining intensity when comparing induction conditions.

These newly described components of RRs are recruited in an ordered manner. Only IMPDH2 was seen in the earliest stages of RR formation, followed by ARL2 recruitment as RRs begin to coalesce into larger structures, and finally calnexin was added at the fully formed RRs (Figures 10 and 11).These data are consistent with a model in which RRs draw from a soluble pool of IMPDH, coalesce, and mature with the addition of the signaling and membrane proteins identified here. The diffuse, cytosolic staining of IMPDH2 seen in untreated cells decreases over time, consistent with relocalization of a large fraction of total cellular IMPDH from the cytosol into RRs (Figure 10), although drawing quantitative conclusions from immunofluorescence data of soluble proteins is challenging. The observation that ARL2 is recruited after initiation of RR formation suggests that it is not required for the initial oligomerization of IMPDH but may play a role in the elongation or stabilization of nascent RRs. The differences in the timing of protein recruitment to RRs and consistency of these differences across the three cell lines tested (HeLa, MEFs, and NRK) suggest that the formation of RRs is a conserved and carefully regulated process.

Two other conditions were also found to induce RR formation—AICAR and glucose starvation—although to various degrees depending on the cell line (Figures 2 and 4). RRs are most often experimentally induced via direct IMPDH binding inhibitors, but they can also be induced by glutamine starvation (Calise *et al.*, 2014), serine starvation, glycine addition (Calise *et al.*, 2016), glutamine analogues (Carcamo *et al.*, 2011; Calise *et al.*, 2014; Keppeke *et al.*, 2015b), and inhibition or knock-down of dihydrofolate reductase (Calise *et al.*, 2016). It is hypothesized that these other inducers of RRs inhibit de novo purine synthesis either by inhibiting enzymes involved in this pathway (glutamine analogues) or by depriving the pathway of necessary substrates (glutamine, serine/glycine). However, purine synthesis inhibition is not necessarily required for RR formation as RRs have been observed following treatments that do not inhibit de novo purine synthesis (Chang *et al.*, 2015; Keppeke *et al.*, 2018) and even under normal growth conditions (Willingham *et al.*, 1987; Gunter *et al.*, 2008; Ramer *et al.*, 2010; Carcamo *et al.*, 2011; Chang *et al.*, 2015). It is possible that alterations in intracellular purine pools (due to interruption of purine synthesis, innate differences in cellular metabolism, or other factors) serve as the trigger for RR formation. To our knowledge, this is the first report of AICAR-mediated induction of RR formation. AICAR is commonly used as an activator of AMP kinase (AMPK). AMPK activation does not appear to be the mechanism of AICAR's effect here because RR formation was independent of AMPK (Figure 3). AICAR is an intermediate in the purine synthesis pathway upstream of IMP. Thus, the robust induction of RRs upon the addition of AICAR may be linked to its role as a metabolite in de novo purine synthesis, possibly by inhibiting the de novo pathway via allosteric inhibition or by altering intracellular purine pools.

Our data further strengthen the links between RR and nucleotide metabolism as we found that guanosine prevents or reverses RR formation (Ji *et al.*, 2006; Calise *et al.*, 2014, 2016) in a process that is dependent on the purine salvage pathway. We have demonstrated that guanosine reverses or prevents RR formation by its conversion to GMP via HGprt in the purine salvage pathway as previously shown (Ji *et al.*, 2006). In previous studies, guanosine always resulted in a complete reversal or prevention of RR formation in all cell lines and RR induction conditions tested (Calise *et al.*, 2014, 2016). Consistent with this, we found that guanosine was capable of reversing RR formation in combination with any of the inducers (MPA, DON, AICAR, and glucose starvation), and in every cell line tested, with the important exception of human fibroblasts lacking functional HGprt (Figure 5 and Supplemental Figures S3 and S4). This demonstrates that RR reversal with guanosine is dependent on HGprt-mediated purine salvage. These results also strengthen the link between RR formation and nucleotide pools, suggesting that RRs form in response to a decrease in guanine nucleotides which guanosine can alleviate via the salvage pathway.

Glucose starvation had the mildest and most variable effect on RR formation in different cell lines compared with other inducers tested (summarized in Table 1). There is one report of glucose depletion inducing CTPS filament (cytoophidia) formation in *Saccharomyces cerevisiae* (Noree *et al.*, 2010), but there are no reports of increases in RRs in mammalian cells. Glucose plays a part in a myriad of metabolic and energetic pathways, offering many ways in which glucose starvation may induce RR formation. Ribose-5-phosphate, generated from glucose via the pentose phosphate pathway, is a precursor for purine nucleotide synthesis. The folate cycle, which has been previously linked to RR formation (Calise *et al.*, 2016), also relies on glucose, as serine, one of the necessary substrates in this cycle, is synthesized from glucose. Overall, these data broaden our understanding of the ways in which RRs can be induced and strengthen the possibility that RRs are linked to other cellular pathways.

The terms RRs and cytoophidia have been used synonymously, and some reports show partial overlap between IMPDH and CTPS in what appear to be a common structure (Ramer *et al.*, 2010; Carcamo *et al.*, 2011, 2014; Keppeke, 2015b). We examined the colocalization between ARL2 and cytoophidia, using CTPS1 as a marker. ARL2 rarely colocalizes with CTPS1 in NRK and IMCD3 cells and never does so in HeLa cells (Figure 6). These results reveal that ARL2 localizes specifically to RRs and highlights a clear difference between RRs and cytoophidia. Although RRs and cytoophidia may be related, most evidence indicates that they are distinct structures. IMPDH inhibitors, the most common method of RR induction, do not induce cytoophidia (Keppeke *et al.*, 2015b). Our results with

MPA induction are in agreement with those findings (Figure 6). Neither glucose starvation nor AICAR induced the formation of cytoophidia, although each led to RR formation. Glutamine analogues such as DON and acivicin induce cytoophidia due to their inhibition of CTPS (Carcamo *et al.*, 2011; Calise *et al.*, 2014; Keppeke *et al.*, 2015a). These drugs also induce the formation of RRs; however, this is likely due to the fact that multiple enzymes involved in de novo purine synthesis require glutamine as a cofactor, making them sensitive to these drugs. Guanosine is capable of reversing RR formation but has no effect on cytoophidia (Keppeke *et al.*, 2015b). Cytoophidia are also smaller than RRs and lack ring-shaped structures (Figure 6). Loukomasomes, another large cellular structure similar in appearance to RRs, have been reported (Noble *et al.*, 2016). However, these structures also appear to be distinct from RRs despite their similar shape. Thus, our data argue strongly that RRs and cytoophidia are not the same structures, although they may have some related roles as both are linked to nucleotide metabolism, which may explain the partial overlap observed between CTPS and IMPDH but not ARL2.

In summary, we describe evidence of the specific, ordered recruitment of ARL2, a subset of its effectors, and ER-derived membranes to RRs. We have recently described roles for ARL2 and TBCD in αβ-tubulin biogenesis (Francis *et al.*, 2017a,b) and for ARL2 and ELMOD2 in mitochondrial fusion (Newman *et al.*, 2014, 2017b), with others demonstrating roles of ARL2 in transport of myristoylated cargo proteins (Jaiswal *et al.*, 2016). Whether any of these processes are linked to RRs is unclear. We speculate that the recruitment of ARL2 and related proteins into RRs could serve a role in inhibiting the actions of this GTPase at other sites via its sequestration into these very large and reversible structures. The specificity with which ARL2, ELMOD2, and cofactor D are each recruited to RRs and the universal roles that regulatory GTPases in the ARF and RAS superfamilies play in cell signaling are consistent with a model linking RRs to some aspect of cell signaling; although we currently lack mechanistic details. With additional components of RRs now elucidated, we are in a better position to understand the function of this fascinating structure and its interaction with cellular organelles.

MATERIALS AND METHODS

Antibodies and reagents

The following antibodies were purchased: Calnexin (Stressgen; SPA-860), GRP78 (Stressgen; SPA-826), SigmaR1 (Abcam; AB89655), CTPS1 (Proteintech Group; 15914-1-AP), Calreticulin (ThermoFisher; PA-900), ELMOD3 (Sigma; HPA012126), TGN46 (Abcam; AB16052), acetylated tubulin (Sigma; 6-11B-1), LC3 (Novus; NB100-2220), α-tubulin (Sigma; T9026), β-tubulin (Sigma; T4026), and HSP60 (Stressgen; ADI-SPA-807). IMPDH2 antibody was raised in rabbit against a peptide representing the FLAP region of IMPDH2 with an N-terminal cysteine appended (CDKHLSSQNRYFSEADKIK). Three mouse monoclonal ARL2 antibodies (3B4.B4, 15E11.B11, and 19F6.F11) were generated by the Emory University mAb core facility using purified bacterially expressed human ARL2 as antigen. Rabbit polyclonal ARL2, ELMOD2, Cofactor D, ARL1, ARL3, ARF1, ARF3, ARF4, ARF6, BART, and ELMOD1 were raised against their corresponding human proteins and have been previously described (Cavenagh *et al.*, 1996; Van Valkenburgh *et al.*, 2001; Sharer *et al.*, 2002; Zhou *et al.*, 2006; Cunningham and Kahn, 2008; East *et al.*, 2012; Newman *et al.*, 2014). Rabbit polyclonal ARL13b antibody was provided by Tamara Caspary (Emory University). The following reagents were purchased: mycophenolic acid (Sigma; M5255), AICAR (Sigma; A9978), DON (Sigma; D2141), 3-methyladenine (Sigma; M9281), bafilomycin (Sigma; B1793), metformin (Combi Blocks; ST-9194), nocodazole (VWR; 102515-934), latrunculin A (Sigma; L5163), cycloheximide (Sigma; 18079), oligomycin (Bio-Chemika; 75352), antimycin A (Sigma; A8674), A-769662 (Abcam; AB120335), guanosine (Sigma; G6264).

Cell lines

The following cell lines were originally obtained from the American Type Culture Collection: HeLa, NRK, IMCD3, MDCK, COS7, G361, and NIH3T3. The control MEFs used throughout these experiments were a generous gift from David Chan (California Institute of Technology; Chen *et al.*, 2003). The AMPK–null MEFs were obtained from B. Viollet (Laderoute *et al.*, 2006). Normal control and HGprt mutant human primary fibroblasts were obtained and cultured as previously described (Fu *et al.*, 2015).

Cell culture

Cells were grown in DMEM (ThermoFisher; 11965) supplemented with 10% fetal bovine serum (FBS; Atlanta Biologicals; S11150) at 37°C in the presence of 5% CO_2. Cells are not cultured beyond 30 passages. Cell density, feeding, and plating schedules were maintained constant between conditions in every experiment, with a target of 70% cell density for data collection. Cells were screened for *Mycoplasma* regularly by staining with Hoechst 33342 DNA dye, usually in conjunction with immunofluorescence experiments.

For glucose-starvation experiments, cells were grown in DMEM and allowed to attach for at least 4 h before exchanging medium. Cells were washed twice with PBS and medium exchanged for no glucose DMEM (ThermoFisher; 11966) supplemented with 10% dialyzed FBS. For MPA induction, cells were treated with 1 µM MPA dissolved in methanol or an equal volume of methanol. For AICAR induction, cells were treated with 1 mM AICAR dissolved in dimethyl sulfoxide (DMSO) or an equal volume of DMSO. For DON experiments, cells were treated with 100 µM DON dissolved in water.

Transfection

Cells at 90% density or higher were transfected in six well plates using a ratio of 2 µg lipofectamine:1 µg DNA. Sec61β plasmid (3 µg) was diluted in 250 µl Opti-MEM (ThermoFisher; 31985). Lipofectamine 2000 (6 µg; ThermoFisher; 11668) was diluted in a separate tube containing 250 µl Opti-MEM, vortexed briefly, and incubated at room temperature for 5 min. The tubes were mixed and incubated for 20 min. Cell culture medium was changed to 1.5 ml of Opti-MEM, and transfection complexes (500 µl) were added dropwise to the cells. After 4 h, cells were trypsinized and replated onto coverslips, typically at a 1:4 split. Cells were fixed and processed for immunofluorescence 24 h after transfection. The plasmid used to drive expression to visualize Sec61β, mCherry-Sec61β, was a gift from Gia Voeltz (University of Colorado; Addgene; #49155).

Immunofluorescence

Cells were grown on matrigel (BD Biosciences; 356231)-coated coverslips. Cells were fixed in a prewarmed (37°C) solution of 4% paraformaldehyde in PBS (140 mM NaCl, 3 mM KCl, 10 mM Na_2HPO_4, 2 mM KH_2PO_4, pH 6.75) for 15 min at room temperature; and permeabilized with 0.1% (vol/vol) Triton X-100 in PBS for 10 min at room temperature. Coverslips were blocked for 1 h at room temperature using filtered PBS containing 1% (wt/vol) bovine serum albumin (BSA; Sigma; A3059). Incubation with primary antibodies was carried out using blocking solution at 4°C overnight, followed by (4 × 5)-min washes in PBS. Secondary antibodies (1:500, Alexa fluorophores;

ThermoFisher) were incubated in blocking solution for 1 h at room temperature. When staining for actin, coverslips were incubated with rhodamine phalloidin (1:1000; ThermoFisher; R415) in conjunction with secondary antibodies. Secondary antibody was removed by (2 × 5)-min washes in PBS. DNA was then stained with Hoechst 33342 for 4 min, followed by (2 × 5)-min washes in PBS and mounting onto slides using Mowiol. Cells are regularly stained with secondary antibody only to ensure specificity of the primary antibodies.

Images were acquired using an Olympus FV1000 microscope and Olympus Fluoview v1.7 software, using 488 and 543 laser excitation and a 100× oil objective (1.45 NA). Z-stacks were acquired with a step size of 0.37 µm, which were converted to maximum image intensity projections using ImageJ where indicated. The following antibody dilutions were used: IMPDH2 (1:10,000), mouse monoclonal ARL2 (1:100), rabbit polyclonal ARL2 (1:2000), ELMOD2 (1:500), cofactor D (1:1000), calnexin (1:1000), GRP78 (1:100), SigmaR1 (1:100), CTPS1 (1:500), calreticulin (1:100), ARL1 (1:1000), ARL3 (1:2000), ARF1 (1:1000), ARF3 (1:1000), ARF4 (1:1000), ARF6 (1:1000), ELMOD1 (1:1000), ELMOD3 (1:500), BART (1:2000), cofactor A (1:1000), cofactor B (1:1000), cofactor C (1:1000), cofactor E (1:1000), TGN46 (1:1000), ARL13b (1:500), acetylated tubulin (1:1000), LC3 (1:200), α-tubulin (1:1000), β-tubulin (1:1000), HSP60 (1:5000).

Antigen competition

Coverslips were prepared for immunofluorescence and primary antibody diluted in blocking solution as described above. More dilute concentrations of primary antibody were used to facilitate competition. Mouse monoclonal ARL2 was used at a dilution of 1:1000, and IMPDH2 was used at a dilution of 1:2,000,000. After antibody was diluted antigen was added at a ratio of 10 µg antigen per 1 µg antibody. For controls, an equal volume of blocking solution was added. The antigen/antibody mixtures and paired controls were incubated for 6 h at 4°C with agitation and then applied to coverslips. Immunofluorescence was then completed as described above.

Purification of human IMPDH2 expressed in *S. cerevisiae* was carried out as described (McPhillips *et al*., 2004) in yeast strain DY3248 (MATa his3Δ1 leu2Δ0 ura3Δ0 MET15 LYS2 Δimd2::LEU2 Δimd3::kanMX4 [pYES2-IMPDH2-TAP (URA3)]) with galactose induction. This strain is deleted for the yeast IMPDH genes and bears a 2µ plasmid with the human IMPDH2 coding region fused to a C-terminal TAP-tag expressed from the yeast GAL1 promoter to allow purification of human IMPDH oligomers free of the yeast proteins. Human ARL2 was purified from bacteria, as described previously (Clark *et al*., 1993).

Electron microscopy

Samples for EM analyses were prepared using standard methods, as described previously (Rizzo *et al*., 2013). In brief, the cells were fixed with 4% paraformaldehyde and 0.05% glutaraldehyde for 30 min at room temperature for immunonanogold labeling or 1% glutaraldehyde for 2 h for morphological analyses. For immunonanogold labeling the cells were permeabilized with 0.1% saponin in blocking solution (PBS containing 1% BSA and 50 mM NH_4Cl) and incubated with antibodies to antigens of interest in the same solution at 4°C overnight (anti-IMPDH2 1:1000 and anti-ARL2 1:10), followed by secondary antibodies labeled with nanogold in the same solution for 2 h at room temperature. The gold particles were then enhanced by nanogold enhancer (Nanoprobes) according to the manufacturer's instructions. The samples were then embedded in epon and ultrathin sections (50–70 nm) were prepared. The samples were examined using a Tecnai 12 120 kV microscope (FEI, The Netherlands). For quantification of the association of RRs with cellular organelles, the criteria used were the following: the membrane of the organelle should be within 20 nm of a RR and the length of this close association should be continuous for at least 50 nm.

Reproducibility/statistics

Every experiment described was independently repeated at least twice in at least three different cell lines. For quantification of immunofluorescence experiments, at least 100 cells per condition were analyzed per experiment. Error bars represent SD.

ACKNOWLEDGMENTS

This work was supported by grants from the National Institutes of Health (NIH; Grant no. GM-122568 to R.A.K.; Grant no. GM-120271 to D.R.). We thank a number of colleagues for their gifts of key reagents used in these studies, including Tamara Caspary (Emory University; Arl13b antibody), David Chan (CalTech; mouse embryonic fibroblasts), Gia Voeltz (University of Colorado at Boulder; plasmid directing expression of mCherry-Sec61β), and Juan Carlos Zabala (Universidad de Cantabria; antibodies to cofactors A/B/C/E). The collection, validation, and distribution of human fibroblasts from LND patients is supported by NIH R56 NS-102980 (H.A.J.). This research project was supported in part by Emory University Integrated Cellular Imaging Microscopy Core of the Emory Neuroscience NINDS Core Facilities Grant no. 5P30NS055077. The EuroBioImaging Facility at the Institute of Protein Biochemistry is funded by grants from MIUR (Ministero dell'Istruzione, dell'Università e della Ricerca), Government of Italy.

REFERENCES

Aguilera-Gomez A, Rabouille C (2017). Membrane-bound organelles versus membrane-less compartments and their control of anabolic pathways in *Drosophila*. Dev Biol 428, 310–317.

Anthony SA, Burrell AL, Johnson MC, Duong-Ly KC, Kuo YM, Simonet JC, Michener P, Andrews A, Kollman JM, Peterson JR (2017). Reconstituted IMPDH polymers accommodate both catalytically active and inactive conformations. Mol Biol Cell 28, 2600–2608.

Aughey GN, Liu JL (2015). Metabolic regulation via enzyme filamentation. Crit Rev Biochem Mol Biol 51, 282–293.

Bailey LK, Campbell LJ, Evetts KA, Littlefield K, Rajendra E, Nietlispach D, Owen D, Mott HR (2009). The structure of binder of Arl2 (BART) reveals a novel G protein binding domain: implications for function. J Biol Chem 284, 992–999.

Bhamidipati A, Lewis SA, Cowan NJ (2000). ADP ribosylation factor-like protein 2 (Arl2) regulates the interaction of tubulin-folding cofactor D with native tubulin. J Cell Biol 149, 1087–1096.

Bole DG, Hendershot LM, Kearney JF (1986). Posttranslational association of immunoglobulin heavy chain binding protein with nascent heavy chains in nonsecreting and secreting hybridomas. J Cell Biol 102, 1558–1566.

Bowzard JB, Cheng D, Peng J, Kahn RA (2007). ELMOD2 is an Arl2 GTPase-activating protein that also acts on Arfs. J Biol Chem 282, 17568–17580.

Calise SJ, Carcamo WC, Krueger C, Yin JD, Purich DL, Chan EK (2014). Glutamine deprivation initiates reversible assembly of mammalian rods and rings. Cell Mol Life Sci 71, 2963–2973.

Calise SJ, Keppeke GD, Andrade LE, Chan EK (2015). Anti-rods/rings: a human model of drug-induced autoantibody generation. Front Immunol 6, 41.

Calise SJ, Purich DL, Nguyen T, Saleem DA, Krueger C, Yin JD, Chan EK (2016). "Rod and ring" formation from IMP dehydrogenase is regulated through the one-carbon metabolic pathway. J Cell Sci 129, 3042–3052.

Carcamo WC, Calise SJ, von Mühlen CA, Satoh M, Chan EKL (2014). Molecular cell biology and immunobiology of mammalian rod/ring structures. Int Rev Cell Mol Biol 308, 35–74.

Carcamo WC, Satoh M, Kasahara H, Terada N, Hamazaki T, Chan JY, Yao B, Tamayo S, Covini G, von Muhlen CA, Chan EK (2011). Induction of cytoplasmic rods and rings structures by inhibition of the CTP and GTP synthetic pathway in mammalian cells. PLoS One 6, e29690.

Carr SF, Papp E, Wu JC, Natsumeda Y (1993). Characterization of human type I and type II IMP dehydrogenases. J Biol Chem 268, 27286–27290.
Cavenagh MM, Whitney JA, Carroll K, Zhang C, Boman AL, Rosenwald AG, Mellman I, Kahn RA (1996). Intracellular distribution of Arf proteins in mammalian cells. Arf6 is uniquely localized to the plasma membrane. J Biol Chem 271, 21767–21774.
Chang CC, Lin WC, Pai LM, Lee HS, Wu SC, Ding ST, Liu JL, Sung LY (2015). Cytoophidium assembly reflects upregulation of IMPDH activity. J Cell Sci 128, 3550–3555.
Charonis AS, Michalak M, Groenendyk J, Agellon LB (2017). Endoplasmic reticulum in health and disease: the 12th International Calreticulin Workshop, Delphi, Greece. J Cell Mol Med 21, 3141–3149.
Chen H, Detmer SA, Ewald AJ, Griffin EE, Fraser SE, Chan DC (2003). Mitofusins Mfn1 and Mfn2 coordinately regulate mitochondrial fusion and are essential for embryonic development. J Cell Biol 160, 189–200.
Chung S, Gumienny TL, Hengartner MO, Driscoll M (2000). A common set of engulfment genes mediates removal of both apoptotic and necrotic cell corpses in *C. ele*gans. Nat Cell Biol 2, 931–937.
Clark J, Moore L, Krasinskas A, Way J, Battey J, Tamkun J, Kahn RA (1993). Selective amplification of additional members of the ADP-ribosylation factor (ARF) family: cloning of additional human and *Drosophila* ARF-like genes. Proc Natl Acad Sci USA 90, 8952–8956.
Colby TD, Vanderveen K, Strickler MD, Markham GD, Goldstein BM (1999). Crystal structure of human type II inosine monophosphate dehydrogenase: implications for ligand binding and drug design. Proc Natl Acad Sci USA 96, 3531–3536.
Covini G, Carcamo WC, Bredi E, von Muhlen CA, Colombo M, Chan EK (2012). Cytoplasmic rods and rings autoantibodies developed during pegylated interferon and ribavirin therapy in patients with chronic hepatitis C. Antivir Ther 17, 805–811.
Cunningham LA, Kahn RA (2008). Cofactor D functions as a centrosomal protein and is required for the recruitment of the gamma-tubulin ring complex at centrosomes and organization of the mitotic spindle. J Biol Chem 283, 7155–7165.
East MP, Bowzard JB, Dacks JB, Kahn RA (2012). ELMO domains, evolutionary and functional characterization of a novel GTPase-activating protein (GAP) domain for Arf protein family GTPases. J Biol Chem 287, 39538–39553.
Francis JW, Goswami D, Novick SJ, Pascal BD, Weikum ER, Ortlund EA, Griffin PR, Kahn RA (2017a). Nucleotide binding to ARL2 in the TBCDARL2β-tubulin complex drives conformational changes in β-tubulin. J Mol Biol 429, 3696–3716.
Francis JW, Newman LE, Cunningham LA, Kahn RA (2017b). A trimer consisting of the tubulin-specific chaperone D (TBCD), regulatory GTPase ARL2, and β-tubulin is required for maintaining the microtubule network. J Biol Chem 292, 4336–4349.
Francis JW, Turn RE, Newman LE, Schiavon C, Kahn RA (2016). Higher order signaling: ARL2 as regulator of both mitochondrial fusion and microtubule dynamics allows integration of 2 essential cell functions. Small Gtpases 7, 188–196.
Fu R, Sutcliffe D, Zhao H, Huang X, Schretlen DJ, Benkovic S, Jinnah HA (2015). Clinical severity in Lesch-Nyhan disease: the role of residual enzyme and compensatory pathways. Mol Genet Metab 114, 55–61.
Gilbert HJ, Lowe CR, Drabble WT (1979). Inosine 5′-monophosphate dehydrogenase of *Escherichia coli*. Purification by affinity chromatography, subunit structure and inhibition by guanosine 5′-monophosphate. Biochem J 183, 481–494.
Gou KM, Chang CC, Shen QJ, Sung LY, Liu JL (2014). CTP synthase forms cytoophidia in the cytoplasm and nucleus. Exp Cell Res 323, 242–253.
Gumienny TL, Brugnera E, Tosello-Trampont AC, Kinchen JM, Haney LB, Nishiwaki K, Walk SF, Nemergut ME, Macara IG, Francis R, *et al*. (2001). CED-12/ELMO, a novel member of the CrkII/Dock180/Rac pathway, is required for phagocytosis and cell migration. Cell 107, 27–41.
Gunter JH, Thomas EC, Lengefeld N, Kruger SJ, Worton L, Gardiner EM, Jones A, Barnett NL, Whitehead JP (2008). Characterisation of inosine monophosphate dehydrogenase expression during retinal development: differences between variants and isoforms. Int J Biochem Cell Biol 40, 1716–1728.
Hebert MD, Poole AR (2017). Towards an understanding of regulating Cajal body activity by protein modification. RNA Biol 14, 761–778.
Ingerson-Mahar M, Briegel A, Werner JN, Jensen GJ, Gitai Z (2010). The metabolic enzyme CTP synthase forms cytoskeletal filaments. Nat Cell Biol 12, 739–746.
Ismail SA, Chen YX, Rusinova A, Chandra A, Bierbaum M, Gremer L, Triola G, Waldmann H, Bastiaens PI, Wittinghofer A (2011). Arl2-GTP and Arl3-GTP regulate a GDI-like transport system for farnesylated cargo. Nat Chem Biol 7, 942–949.
Ivanova AA, East MP, Yi SL, Kahn RA (2014). Characterization of recombinant ELMOD (cell engulfment and motility domain) proteins as GTPase-activating proteins (GAPs) for ARF family GTPases. J Biol Chem 289, 11111–11121.
Jaiswal M, Fansa EK, Kösling SK, Mejuch T, Waldmann H, Wittinghofer A (2016). Novel biochemical and structural insights into the interaction of myristoylated cargo with Unc119 and their release by Arl2/3. J Biol Chem 291, 20766–20778.
Ji Y, Gu J, Makhov AM, Griffith JD, Mitchell BS (2006). Regulation of the interaction of inosine monophosphate dehydrogenase with mycophenolic acid by GTP. J Biol Chem 281, 206–212.
Juda P, Smigova J, Kovacik L, Bartova E, Raska I (2014). Ultrastructure of cytoplasmic and nuclear inosine-5′-monophosphate dehydrogenase 2 "rods and rings" inclusions. J Histochem Cytochem 62, 739–750.
Keppeke GD, Andrade LE, Grieshaber SS, Chan EK (2015a). Microinjection of specific anti-IMPDH2 antibodies induces disassembly of cytoplasmic rods/rings that are primarily stationary and stable structures. Cell Biosci 5, 1.
Keppeke GD, Calise SJ, Chan EK, Andrade LE (2015b). Assembly of IMPDH2-based, CTPS-based, and mixed rod/ring structures is dependent on cell type and conditions of induction. J Genet Genomics 42, 287–299.
Keppeke GD, Chang CC, Peng M, Chen LY, Lin WC, Pai LM, Andrade LEC, Sung LY, Liu JL (2018). IMP/GTP balance modulates cytoophidium assembly and IMPDH activity. Cell Div 13, 5.
Keppeke GD, Nunes E, Ferraz ML, Silva EA, Granato C, Chan EK, Andrade LE (2012). Longitudinal study of a human drug-induced model of autoantibody to cytoplasmic rods/rings following HCV therapy with ribavirin and interferon-α. PLoS One 7, e45392.
Keppeke GD, Prado MS, Nunes E, Perazzio SF, Rodrigues SH, Ferraz ML, Chan EK, Andrade LE (2016). Differential capacity of therapeutic drugs to induce rods/rings structures in vitro and in vivo and generation of anti-rods/rings autoantibodies. Clin Immunol 173, 149–156.
Klinger CM, Spang A, Dacks JB, Ettema TJ (2016). Tracing the archaeal origins of eukaryotic membrane-trafficking system building blocks. Mol Biol Evol 33, 1528–1541.
Laderoute KR, Amin K, Calaoagan JM, Knapp M, Le T, Orduna J, Foretz M, Viollet B (2006). 5′-AMP-activated protein kinase (AMPK) is induced by low-oxygen and glucose deprivation conditions found in solid-tumor microenvironments. Mol Cell Biol 26, 5336–5347.
Li Y, Kelly WG, Logsdon JM Jr, Schurko AM, Harfe BD, Hill-Harfe KL, Kahn RA (2004). Functional genomic analysis of the ADP-ribosylation factor family of GTPases: phylogeny among diverse eukaryotes and function in *C. elegans*. FASEB J 18, 1834–1850.
Liu JL (2011). The enigmatic cytoophidium: compartmentation of CTP synthase via filament formation. Bioessays 33, 159–164.
Liu JL (2016). The cytoophidium and its kind: filamentation and compartmentation of metabolic enzymes. Annu Rev Cell Dev Biol 32 349–372.
Liu F, Jin R, Liu X, Huang H, Wilkinson SC, Zhong D, Khuri FR, Fu H, Marcus A, He Y, Zhou W (2016). LKB1 promotes cell survival by modulating TIF-IA-mediated pre-ribosomal RNA synthesis under uridine downregulated conditions. Oncotarget 7, 2519–2531.
Logsdon JM Jr, Kahn RA (2004). The Arf Family Tree. In: Arf Family GTPases, ed. R. A. Kahn, pp. 1–22, Dordrecht, Netherlands: Kluwer Academic Publishers.
Luo Y, Na Z, Slavoff SA (2018). P-bodies: composition, properties, and functions. Biochemistry 57), 2424–2431.
McPhillips CC, Hyle JW, Reines D (2004). Detection of the mycophenolate-inhibited form of IMP dehydrogenase in vivo. Proc Natl Acad Sci USA 101, 12171–12176.
Muromoto R, Sekine Y, Imoto S, Ikeda O, Okayama T, Sato N, Matsuda T (2008). BART is essential for nuclear retention of STAT3. Int Immunol 20, 395–403.
Newman LE, Schiavon CR, Turn RE, Kahn RA (2017a). The ARL2 GTPase regulates mitochondrial fusion from the intermembrane space. Cell Logist 7, e1340104.
Newman LE, Schiavon CR, Zhou C, Kahn RA (2017b). The abundance of the ARL2 GTPase and its GAP, ELMOD2, at mitochondria are modulated by the fusogenic activity of mitofusins and stressors. PLoS One 12, e0175164.
Newman LE, Zhou CJ, Mudigonda S, Mattheyses AL, Paradies E, Marobbio CM, Kahn RA (2014). The ARL2 GTPase is required for mitochondrial morphology, motility, and maintenance of ATP levels. PLoS One 9, e99270.

Noble JW, Hunter DV, Roskelley CD, Chan EK, Mills J (2016). Loukoumasomes are distinct subcellular structures from rods and rings and are structurally associated with MAP2 and the nuclear envelope in retinal cells. PLoS One 11, e0165162.
Noree C, Sato BK, Broyer RM, Wilhelm JE (2010). Identification of novel filament-forming proteins in *Saccharomyces cerevisiae* and *Drosophila melanogaster*. J Cell Biol 190, 541–551.
Nunez Villacis L, Wong MS, Ferguson LL, Hein N, George AJ, Hannan KM (2018). New roles for the nucleolus in health and disease. Bioessays 40, e1700233.
Pinkus LM (1977). Glutamine binding sites. Methods Enzymol 46, 414–427.
Ramer MS, Cruz Cabrera MA, Alan N, Scott AL, Inskip JA (2010). A new organellar complex in rat sympathetic neurons. PLoS One 5, e10872.
Rizzo R, Parashuraman S, Mirabelli P, Puri C, Lucocq J, Luini A (2013). The dynamics of engineered resident proteins in the mammalian Golgi complex relies on cisternal maturation. J Cell Biol 201, 1027–1036.
Ruscher K, Wieloch T (2015). The involvement of the sigma-1 receptor in neurodegeneration and neurorestoration. J Pharmacol Sci 127, 30–35.
Russell RR 3rd, Bergeron R, Shulman GI, Young LH (1999). Translocation of myocardial GLUT-4 and increased glucose uptake through activation of AMPK by AICAR. Am J Physiol 277(2 Pt 2), H643–H649.
Seelig HP, Appelhans H, Bauer O, Bluthner M, Hartung K, Schranz P, Schultze D, Seelig CA, Volkmann M (2011). Autoantibodies against inosine-5′-monophosphate dehydrogenase 2—characteristics and prevalence in patients with HCV-infection. Clin Lab 57, 753–765.
Sharer JD, Kahn RA (1999). The ARF-like 2 (ARL2)-binding protein, BART. Purification, cloning, and initial characterization. J Biol Chem 274, 27553–27561.
Sharer JD, Shern JF, Van Valkenburgh H, Wallace DC, Kahn RA (2002). ARL2 and BART enter mitochondria and bind the adenine nucleotide transporter. Mol Biol Cell 13, 71–83.
Shern JF, Sharer JD, Pallas DC, Bartolini F, Cowan NJ, Reed MS, Pohl J, Kahn RA (2003). Cytosolic Arl2 is complexed with cofactor D and protein phosphatase 2A. J Biol Chem 278, 40829–40836.
Suzuki M, Murakami T, Cheng J, Kano H, Fukata M, Fujimoto T (2015). ELMOD2 is anchored to lipid droplets by palmitoylation and regulates adipocyte triglyceride lipase recruitment. Mol Biol Cell 26, 2333–2342.
Thomas EC, Gunter JH, Webster JA, Schieber NL, Oorschot V, Parton RG, Whitehead JP (2012). Different characteristics and nucleotide binding properties of inosine monophosphate dehydrogenase (IMPDH) isoforms. PLoS One 7, e51096.
Tian G, Huang Y, Rommelaere H, Vandekerckhove J, Ampe C, Cowan NJ (1996). Pathway leading to correctly folded β-tubulin. Cell 86, 287–296.
Tsai YL, Ha DP, Zhao H, Carlos AJ, Wei S, Pun TK, Wu K, Zandi E, Kelly K, Lee AS (2018). Endoplasmic reticulum stress activates SRC, relocating chaperones to the cell surface where GRP78/CD109 blocks TGF-β signaling. Proc Natl Acad Sci USA 115, E4245–E4254.
Van Valkenburgh H, Shern JF, Sharer JD, Zhu X, Kahn RA (2001). ADP-ribosylation factors (ARFs) and ARF-like 1 (ARL1) have both specific and shared effectors: characterizing ARL1-binding proteins. J Biol Chem 276, 22826–22837.
Watzlich D, Vetter I, Gotthardt K, Miertzschke M, Chen YX, Wittinghofer A, Ismail S (2013). The interplay between RPGR, PDEδ and Arl2/3 regulate the ciliary targeting of farnesylated cargo. EMBO Rep 14, 465–472.
Whitby FG, Luecke H, Kuhn P, Somoza JR, Huete-Perez JA, Phillips JD, Hill CP, Fletterick RJ, Wang CC (1997). Crystal structure of *Tritrichomonasfoetus* inosine-5′-monophosphate dehydrogenase and the enzyme-product complex. Biochemistry 36, 10666–10674.
Wiest DL, Bhandoola A, Punt J, Kreibich G, McKean D, Singer A (1997). Incomplete endoplasmic reticulum (ER) retention in immature thymocytes as revealed by surface expression of "ER-resident" molecular chaperones. Proc Natl Acad Sci USA 94, 1884–1889.
Wiest DL, Burgess WH, McKean D, Kearse KP, Singer A (1995). The molecular chaperone calnexin is expressed on the surface of immature thymocytes in association with clonotype-independent CD3 complexes. EMBO J 14, 3425–3433.
Willingham MC, Richert ND, Rutherford AV (1987). A novel fibrillar structure in cultured cells detected by a monoclonal antibody. Exp Cell Res 171, 284–295.
Zhang T, Li S, Zhang Y, Zhong C, Lai Z, Ding J (2009). Crystal structure of the ARL2-GTP-BART complex reveals a novel recognition and binding mode of small GTPase with effector. Structure 17, 602–610.
Zhou C, Cunningham L, Marcus AI, Li Y, Kahn RA (2006). Arl2 and Arl3 regulate different microtubule-dependent processes. Mol Biol Cell 17, 2476–2487.